SAR Image Registration Using Phase Congruency and Nonlinear Diffusion-Based SIFT

Jianwei Fan, Yan Wu, Fan Wang, Qiang Zhang, Guisheng Liao, and Ming Li

***Abstract*—The scale-invariant feature transform (SIFT) algorithm has been widely applied to optical image registration. However, mostly because of multiplicative speckle noise, SIFT has a limited performance when directly applied to synthetic aperture radar (SAR) image. In this letter, a novel SAR image registration method is proposed, which is based on the combination of SIFT, nonlinear diffusion, and phase congruency. In our proposed algorithm, the multiscale representation of a SAR image is generated by nonlinear diffusion, since it better preserves edges in the image as opposed to Gaussian smoothing, which is used in the original SIFT. To reduce the influence of multiplicative speckle noise, the ratio of exponential weighted average operator is used to compute the gradient information in the construction of nonlinear diffusion scale space. Moreover, phase congruency information is utilized to remove the erroneous keypoints within the initial keypoints. Experimental results on multipolarization, multiband, and multitemporal SAR images indicate that our algorithm can improve the match performance compared to the SIFT-based method, which leads to a subpixel accuracy for all the tested image pairs.**

***Index Terms*—Nonlinear diffusion, phase congruency, scale-invariant feature transform (SIFT), synthetic aperture radar (SAR) image registration.**

I. Introduction

SYNTHETIC aperture radar (SAR) is a coherent imaging system, which can produce high-resolution images and work under all time and all weather conditions. Hence, it is useful for diverse applications, including image fusion, environmental surveillance, change detection [1], and so on. As a fundamental step required by these applications, image registration refers to the alignment of images of the same scene obtained under different imaging conditions, such as at different times, from different viewpoints, or by different sensors.

Recently, due to its invariances to scale changes, rotations, translations and partially to illumination and viewpoint changes, scale-invariant feature transform (SIFT) has been widely applied to many image processing tasks. Based on the multiscale representation of an image (i.e., a series of difference-of-Gaussian (DoG) images), SIFT detects keypoints, by searching extremal values in the DoG pyramid, and then computes a keypoint descriptor in the local image patches around each keypoint. The descriptor encodes the spatial gradient distribution around a keypoint by a 128-dimensional vector, which is used for the following match. More details about SIFT can be referred to [2].

Although SIFT has been successfully applied to optical image registration, owing to its distinctiveness in feature description, it may not produce satisfying results when directly applied to SAR images [3]. The reasons may consist of two aspects. First, SAR images are usually corrupted by strong multiplicative speckle noises, which deteriorate SIFT for keypoint extraction. Therefore, many incorrect keypoints may appear with the SIFT method [4], [5]. Second, the Gaussian scale space (GSS) used in SIFT often degrades edge information and fine details in the image as a result of the Gaussian smoothing operation [6]. Due to the defects of losing details, blurring edges, and its weak speckle noise immunity, SIFT will obtain many erroneous initial keypoints from DoG, when dealing with SAR image registration. After removal of these outliers, correct matches available are too insufficient for us to calculate transformation parameters. In this case, SIFT fails.

To overcome the problems aforementioned, nonlinear diffusion is utilized in this letter to generate the scale space [i.e., nonlinear diffusion scale space (NDSS)], which has an advantage of preserving edges and details over the linear GSS [7], [8]. Meanwhile, the ratio of exponential weighted average (ROEWA) operator is used to compute the gradient information during the construction of NDSS. In addition, the obtained initial keypoints are refined by exploring their phase congruency information. Compared with the SIFT-based method, the proposed approach is competent to the problem of SAR image registration, as shown by our experiments.

The rest of this letter is organized as follows: The proposed SAR image registration approach is introduced in Section II, with emphasis on the generation of NDSS and the procedure of outlier removal, and the experimental results of the proposed algorithm and other registration methods are presented and compared in Section III. Concluding remarks are given in Section IV.

II. SAR Image Registration Using Phase Congruency and Nonlinear Diffusion-Based SIFT

Here, the improved SIFT for SAR image registration is introduced in detail. In comparison with the original SIFT algorithm, the proposed method focuses on the following improvements: 1) utilizing nonlinear diffusion to generate the scale space in the improved SIFT; 2) introducing a robust approach to compute

Manuscript received May 28, 2014; revised July 16, 2014 and July 28, 2014; accepted August 19, 2014. This work was supported by the Natural Science Foundation of China under Grant 61272281 and Grant 61271297, by the National Key Basic Research and Development Program of China (973) under Grant 2011CB707001, by the National Defense Foundation of China under Grant 9140A07020913DZ01001, and by the Fundamental Research Funds for the Central Universities under Grant 7214314702 and Grant 7214588502.

J. Fan, Y. Wu, F. Wang, and Q. Zhang are with Remote Sensing Image Processing and Fusion Group, School of Electronic Engineering, Xidian University, Xi'an 710071, China (e-mail: ywu@mail.xidian.edu.cn).

G. Liao and M. Li is with the National Key Laboratory of Radar Signal Processing, Xidian University, Xi'an 710071, China.

Color versions of one or more of the figures in this paper are available online at http://ieeexplore.ieee.org.

Digital Object Identifier 10.1109/LGRS.2014.2351396

the gradient information involved in the NDSS for SAR image; and 3) providing an outlier removal stage that is based on the phase congruency information. Details will be elaborated in the following subsections.

A. Creation of Scale Space With Nonlinear Diffusion

The GSS used in the SIFT method is produced from the convolution of the original image with Gaussian filters at different scales [2]. Gaussian smoothing has the effect of denoising; however, some important fine details in the image may be lost as well, which will have a bad effect on feature detection.

To make up for the defect of GSS, the multiscale representation of SAR image is generated using nonlinear diffusion equation described in [9], which is defined as

$$\begin{aligned}\frac{\partial f(x,y)}{\partial t} &= f_t = \operatorname{div}\left(c(x,y,t)\nabla f\right)\\ &= c(x,y,t)\Delta f + \nabla c \cdot \nabla f \end{aligned} \tag{1}$$

where t is the scale parameter; div is the divergence operator; ∇ and Δ are the gradient and Laplacian operators, respectively; $c(x,y,t)$ is the diffusion coefficient. It reduces to isotropic diffusion equation if $c(x,y,t)$ is a constant, which is equivalent to Gaussian smoothing.

The diffusion coefficient $c(x,y,t)$ is generally regarded as a nonlinear function of the image gradient $|\nabla f|$, and two different formulations for the diffusion coefficients are introduced in [9]

$$c_1 = e^{\left(-\left(\frac{|\nabla f|}{K}\right)^2\right)} \tag{2}$$

$$c_2 = \frac{1}{1+\left(\frac{|\nabla f|}{K}\right)^2}. \tag{3}$$

The parameter K is the contrast factor that controls the level of diffusion, and it determines which edges have to be kept or cancelled. The greater the K value is, the less edge information will be preserved. The K value can be either empirically fixed or estimated from the image gradient histogram [6].

Furthermore, the scale spaces generated by these two coefficients are different: the former prefers to enhance high-contrast edges rather than low-contrast ones, and the latter privileges wide regions over smaller ones. From its definition as a monotone decreasing function of the image gradient, it is obvious that the diffusion coefficient with a smaller gradient value diffuses much more quickly than that with a larger gradient value. Based on this principle, edges in an image will be preserved. In this letter, c_2 is taken as the diffusion coefficient.

Since there are no analytical solutions for solving the nonlinear diffusion equation [i.e., (1)], one needs to approximate the solution using a numerical method. A computationally efficient solution for (1) was proposed by Weickert *et al.* [10], where the additive operator splitting (AOS) scheme is used. Applying the AOS scheme in (1) yields the following relationship:

$$f^{k+1} = \left(I - \tau \sum_{l=1}^{m} A_l(f^k)\right)^{-1} f^k. \tag{4}$$

Here, τ denotes the time step, I is the identity matrix, l denotes the direction, and the matrix A_l corresponds to derivatives along the lth coordinate axis. More details about how to build the matrix A_l can be found in [10]. The equation earlier requires solving a linear system problem, where the system matrix is tridiagonal and diagonal dominant. Fortunately, by means of the Thomas algorithm, this issue can be solved efficiently.

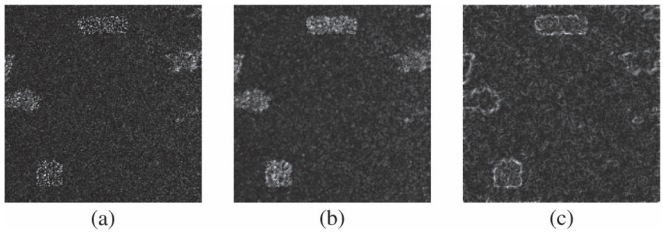

Fig. 1. Results of two gradient computation methods. (a) Image corrupted with speckle noise. (b) Gradient obtained by first-order differencing method. (c) Gradient obtained by ROEWA (after contrast stretched).

During the creation of NDSS, gradient information within an image is required. Normally, the gradient can be obtained by the simple first-order differencing method. However, due to multiplicative speckle noise, this method is not suitable for SAR image. It will produce false edges in the areas with high reflectivity and lose some image information in the ones with low reflectivity [4].

Considering the influence of speckle noise in gradient information calculation, ROEWA is introduced owing to its advantage of possessing constant false alarm rate and robustness against speckle noise over the first-order differencing method [11]. To better illustrate the difference between the first-order differencing method and ROEWA, Fig. 1 presents the gradient magnitude on an image corrupted by speckle noise through the two gradient computation methods. Clearly, the gradient computed by the first-order differencing method produces larger values in high reflectivity areas than in low reflectivity ones, whereas the gradient obtained with ROEWA makes slight difference on homogeneous areas under different reflectivity conditions. Due to its robustness against speckle noise, ROEWA is utilized to compute the gradient information in the creation of NDSS. By doing so, we can produce a scale space that has a better robustness to speckle noise.

We take the same approach as done in SIFT, discretizing the scale space into a series of O octaves and S sublevels. The multiscale representation of a SAR image is generated as a stack of smoothed images, with the original image as a condition and scale values being equal to $t = \sigma^2/2$ [12], where σ values are calculated from the following expression:

$$\sigma_i(o,s) = \sigma_0 2^{o+\frac{s}{S}}, o \in [0,\ldots,O-1], s \in [0,\ldots,S+2, \quad i \in [0,\ldots,W-1] \tag{5}$$

where σ_0 is the base scale level, and W is the total number of the smoothed images; o and s are the index of octave O and sublevel S, respectively. It is noteworthy that, when we reach the last sublevel in each octave, we downsample the image, as described in SIFT, and use the downsample image as the initial image for the next octave. Meanwhile, to achieve better information preservation in SAR image, the contrast factor K should be modified after each downsample. The procedure of multiscale representation by nonlinear diffusion is outlined in Algorithm 1.

TABLE I
PRIOR INFORMATION OF THE REAL SAR IMAGES

SAR Images		Sensor	Spatial Resolution	Band	Polarization	Size	Date of Acquisition	Location of Acquisition
Dataset1	Ref. image	PISAR	3m	L	HH	320×320	1999/10/14	Niigata Site
	Sen. image	PISAR	3m	L	HV	320×320	1999/10/14	Niigata site
Dataset2	Ref. image	AIRSAR	10m	L	HH	374×374	2003/03/30	Rabbit Ears
	Sen. image	AIRSAR	10m	C	HH	306×306	2003/03/30	Rabbit Ears
Dataset3	Ref. image	ERS-2	30m	C	VV	340×340	1996/06/04	Shanghai
	Sen. image	ERS-2	30m	C	VV	300×300	2002/04/09	Shanghai

Algorithm 1 Multiscale representation procedure by nonlinear diffusion

Input: image f^0, contrast factor K, scale level σ_i
for $i = 0 \rightarrow W - 1$ **do**

1) Compute scale value t_i.
2) Deduce diffusion coefficient c based on image gradient $|\nabla f|$ obtained with ROEWA.
3) Compute matrix $A_l(f^i)$.
4) Update iteratively f according to (6) based on AOS scheme:

$$f^{i+1} = \left(I - (t_{i+1} - t_i) \sum_{l=1}^{m} A_l(f^i) \right)^{-1} f^i \tag{6}$$

if $o_{i+1} > o_i$ **then**
Downsample the image f^i, and modify contrast factor K value.
end if
end for
Output: a stack of smoothed images $f^i, i = 0, \ldots, W - 1$

Based on the method that we present for generating NDSS, the obtained multiscale images are able to better preserve edges and details and be more robust against speckle noise. Therefore, with the NDSS, the improved SIFT is expected to detect much more keypoints. Once the smoothed images at different scales have been generated, the difference between adjacent scales is performed, and the steps of feature detection and description follow those used in SIFT algorithm.

B. Outlier Removal Using Phase Congruency

Due to the existence of multiplicative speckle noise, a large number of unreliable keypoints appear within the initial keypoints detected by our approach. These unreliable matches will lead to inaccurate correspondences and further affect the correct calculation of the transformation parameters. With this in view, we have attempted to introduce phase congruency to eliminate the outliers. It has been shown that phase congruency is invariant to illumination and contrast condition. The phase congruency information in the image is obtained by analyzing the logarithmic Gabor filter responses over different orientations and scales [13]. The outlier removal in this letter is accomplished with the following steps:

1) Compute phase congruency information at each point in the reference and sensed images; the corresponding phase congruency information can be defined as

$$P(x,y) = \frac{\sum_n W(x,y) \lfloor A_n(x,y) \Delta\phi_n(x,y) - T \rfloor}{\sum_n A_n(x,y) + \varepsilon} \tag{7}$$

$$\Delta\phi_n(x,y) = \cos\left(\phi_n(x,y) - \bar{\phi}(x,y)\right) - \left|\sin\left(\phi_n(x,y) - \bar{\phi}(x,y)\right)\right| \tag{8}$$

where (x, y) indicates the coordinate of a point, and subscript n is the scale of the filter. $W(x, y)$ is the weighting factor based on frequency spread, and $A_n(x, y)$ and $\phi_n(x, y)$ are the amplitude and phase at scale n, respectively. $\bar{\phi}(x, y)$ is the weighted mean phase, T is the noise threshold, and ε is a small constant to avoid division by zero.
2) For the SAR image, phase congruency at a noise or unreliable site is relatively weaker than that at a correct site. If the phase congruency information at a keypoint (denoted by P_i) is larger than a threshold, i.e., $P_i \geq th$, then the point is validated. If P_i is below th, then the point is rejected, where th is a preset threshold, and an empirical value of 0.01 is suggested.

Following the two steps aforementioned will remove many erroneous keypoints, which is expected to improve the probability of correct matching. After the removal of the outliers using phase congruency, we use minimum Euclidean distance on the descriptor vector for each keypoint to find its corresponding point. The ratio between the distance of the closest neighbor and the distance to the second closest neighbor is calculated to exclude false matches. Regarding the value of the distance ratio, 0.8 is preferred by Lowe [2]. Moreover, we utilize the dual-matching strategy proposed in [7] to further select correct matches, i.e., reference keypoint A and keypoint B in the sensed image are considered as a correspondence only when the two points are matched to each other by the distance ratio.

III. EXPERIMENTAL RESULTS AND ANALYSIS

To evaluate the performance of the proposed algorithm, we experimentally validate it on several pairs of real SAR images, and the corresponding prior information of SAR images are shown in Table I. In Section III-A, the multiscale representations of SAR images are displayed to verify the effectiveness of our NDSS combined with ROEWA. In Section III-B, the registration comparisons between the proposed method and others are implemented to demonstrate the superiority of our methodology in registration performance.

A. Performance of NDSS

Here, a brief comparison of NDSS with GSS is given. We construct the multiscale representation of a SAR image using

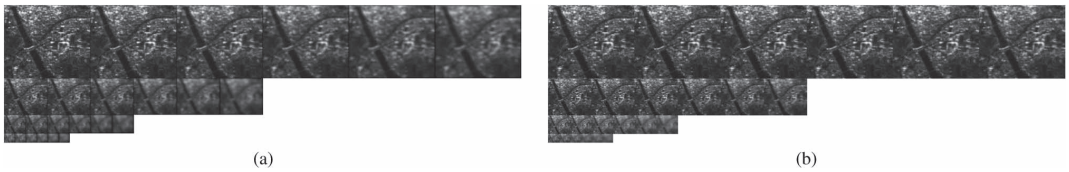

Fig. 2. Comparison between GSS and NDSS at the same scales. (a) GSS images with four octaves and six sublevels within each octave. (b) NDSS images with four octaves and six sublevels within each octave.

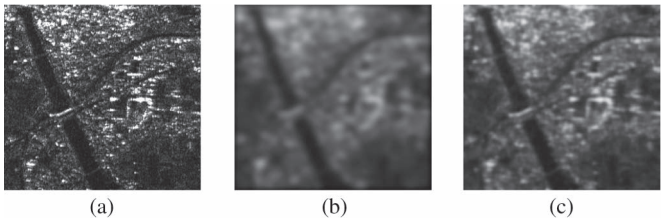

Fig. 3. Comparison of GSS with our scale space. (a) Original SAR image. (b) GSS image. (c) NDSS image.

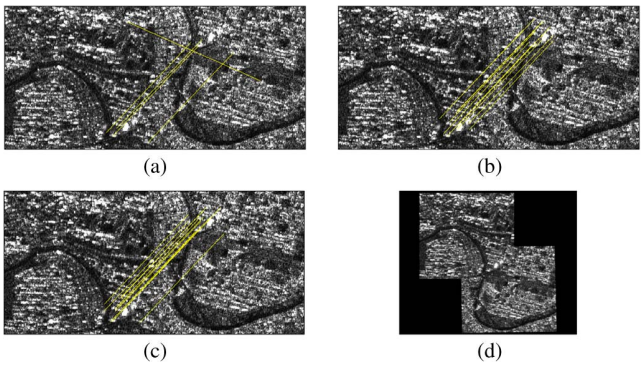

Fig. 4. Matches found in data set 1 using (a) BFSIFT, (b) SIFT+NDSS, and (c) our proposed approach. The reference image is shown on the left and the sensed image on the right. (d) Registration result by our proposed approach.

nonlinear diffusion and Gaussian smoothing, respectively. The results are illustrated in Fig. 2, where the images on the left [i.e., Fig. 2(a)] are produced by GSS, and the images on the right [i.e., Fig. 2(b)] are the nonlinear version with the same scales. In this letter, we use the same number of octaves $O = 4$ and sublevels $S = 3$, for all the methods.

As shown in Fig. 2, the difference between NDSS and GSS is apparent. While the GSS images are increasingly blurred with increasing scale values, the nonlinear ones have a relatively slight or small blurriness, which will contribute to extract more keypoints. For a better visual illustration, a more detailed description is presented. The two images in Fig. 3 are both at the fourth sublevel within the second octave. As it can be observed in Fig. 3, NDSS exhibits its advantage in comparison with GSS.

The image smoothed by Gaussian filter is more blurred, and its edges and details disappear because of Gaussian blurring, whereas the NDSS image can better preserve edges and details.

B. Comparison With Other Image Registration Methods

Here, three pairs of real SAR images are utilized to validate our approach in terms of effectiveness and accuracy, and the transformation difference of the two images in each image pair consists mainly of translation, rotation, and scale, which are modeled by the affine transformation. The proposed method is compared with two other approaches. The bilateral filter scale-invariant feature transform (BFSIFT) algorithm [7]

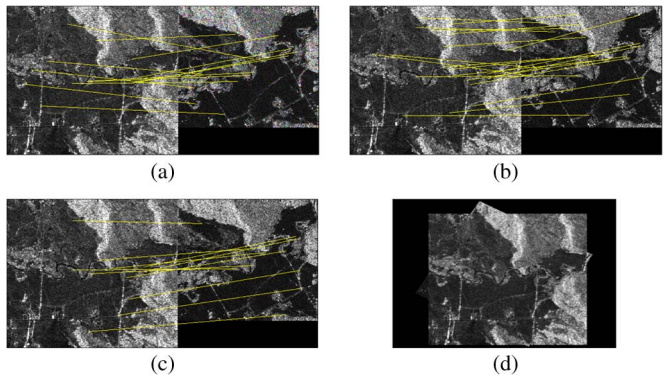

Fig. 5. Matches found in data set 2 using (a) BFSIFT, (b) SIFT+NDSS, and (c) our proposed approach. The reference image is shown on the left and the sensed image on the right. (d) Registration result by our proposed approach.

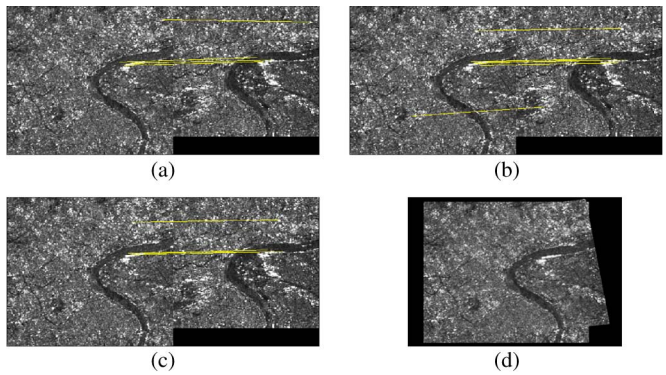

Fig. 6. Matches found in data set 3 using (a) BFSIFT, (b) SIFT+NDSS, and (c) our proposed approach. The reference image is shown on the left and the sensed image on the right. (d) Registration result by our proposed approach.

is considered as the first method for comparison, whereas SIFT+NDSS is the second considered method. SIFT+NDSS here refers to the multiscale representation method by applying NDSS to SIFT instead of the original GSS. A comparison between SIFT+NDSS and our approach is used for illustrating the performance of our outlier removal procedure.

1) Data Set 1—Images From Different Polarizations: This pair of images is obtained from Japan's polarimetric and interferometric airborne synthetic aperture radar (PISAR) system. The matches found in data set 1 using the three methods mentioned earlier are shown in Fig. 4.

2) Data Set 2—Images From Different Wavelengths: The second considered pair of images is composed by two airborne synthetic aperture radar (AIRSAR) (an airborne SAR sensor used by the National Aeronautics and Space Administration/Jet Propulsion Laboratory) scenes. The matches obtained in data set 2 using the three methods described earlier are shown in Fig. 5.

3) Data Set 3—Images From Different Times: In this part, we choose a data set from multitemporal scenes acquired by

TABLE II
QUANTITATIVE COMPARISON OF THE PROPOSED METHOD WITH BFSIFT AND SIFT+NDSS (∗ THE FIRST NUMBER INDICATES THE KEYPOINTS OBTAINED AFTER THE REMOVAL OF THE OUTLIERS USING PHASE CONGRUENCY)

SAR images	method	Number of keypoints			RMSE/pixel	RMS_{LOO} /pixel	time/s
		Reference image	Sensed image	Match			
Dataset1	BFSIFT	1940	1902	5	8.35	5.42	45.79
	SIFT+NDSS	3237	3291	12	1.17	1.14	39.52
	Our approach	1914/3237 *	1807/3291	12	0.81	0.83	39.04
Dataset2	BFSIFT	556	335	14	24.47	23.06	41.12
	SIFT+NDSS	793	440	20	2.89	2.86	13.53
	Our approach	337/793	230/440	11	0.94	0.95	16.61
Dataset3	BFSIFT	590	503	4	0.95	0.97	38.72
	SIFT+NDSS	796	648	6	0.65	0.70	13.29
	Our approach	578/796	499/648	4	0.49	0.51	15.85

the European Remote Sensing Satellite 2 (ERS-2). The matches found in data set 3 using the three methods mentioned earlier are presented in Fig. 6.

To quantitatively evaluate the registration performances, we adopt the root-mean-square error (RMSE) between the corresponding matching keypoints, and it can be expressed as

$$\text{RMSE} = \sqrt{\frac{1}{n}\sum_{i=1}^{n}(x_i - x_i')^2 + (y_i - y_i')^2} \tag{9}$$

where (x_i, y_i) and (x_i', y_i') are the coordinates of the ith matching keypoint pair; n means the total number of matching points. In addition, another effective measure described in [14] is used, hereafter assigned as RMS_{LOO}. Based on the leave-one-out method, the RMS_{LOO} measure is regarded as a much more fair measure. With respect to RMSE and RMS_{LOO}, the accuracy of subpixel is satisfactory. The quantitative evaluation results for each method are listed in Table II.

Of the three methods used for comparison, our proposed approach gives the best performance among the comparisons. By visual inspection, it appears that the registration results [i.e., Figs. 4(d)–6(d)] are valid and accurate in all data sets. In Figs. 4–6 and Table II, we make the following observations: 1) Except data set 3, two other data sets cannot be registered successfully by the BFSIFT method due to the existence of erroneous matches, as presented in Figs. 4(a) and 5(a). 2) The NDSS-based method can extract more keypoints than the BFSIFT method. With respect to the running time (all timing results are obtained on a 2.7-GHz PC), our approach clearly outperformed the BFSIFT method. 3) Although SIFT+NDSS has achieved better registration performance in contrast to the BFSIFT method on SAR image, it would lead to a relatively large value of RMSE, which is an unacceptable result. 4) In comparison with BFSIFT, our method not only obtains more number of the initial keypoints but also has a much higher matching accuracy. Meanwhile, our method outperforms SIFT+NDSS in terms of matching accuracy. This advantage stems from our outlier removal stage with phase congruency information, which eliminates those erroneous keypoints.

Overall, the advantage of our approach can be seen qualitatively and quantitatively by referring to Figs. 4–6 and Table II. The aligning accuracy of our proposed method is within one pixel.

IV. CONCLUSION

In this letter, a novel algorithm for SAR image registration has been proposed, which combines SIFT, nonlinear diffusion, and phase congruency. In our algorithm, NDSS with ROEWA is used for representing the multiscale of the SAR images, and it effectively reduces the speckle noise and preserves fine details in the image simultaneously. ROEWA is used to compute the gradient in our creation of scale space, and its advantages have been experimentally demonstrated on the image. Finally, phase congruency information at each keypoint is used as a cue for rejecting the false keypoints.

A comparison of the proposed method with the SIFT+NDSS and BFSIFT method is given, and the result has shown that the number of keypoints obtained using our approach is more than that by BFSIFT with bilateral filter. Moreover, by analyzing the phase congruency information of keypoints, our method has a remarkable improvement in match accuracy.

REFERENCES

[1] F. Wang *et al.*, "Unsupervised change detection on SAR images using triplet Markov field model," *IEEE Geosci. Remote Sens. Lett.*, vol. 10, no. 4, pp. 697–701, Jul. 2013.

[2] D. G. Lowe, "Distinctive image features form scale-invariant keypoints," *Int. J. Comput. Vis.*, vol. 60, no. 2, pp. 91–110, Nov. 2004.

[3] H. Goncalves, L. Corte-Real, and J. A. Goncalves, "Automatic image registration through image segmentation and SIFT," *IEEE Trans. Geosci. Remote Sens.*, vol. 49, no. 7, pp. 2589–2600, Jul. 2011.

[4] F. Dellinger, J. Delon, Y. Gousseau, J. Michel, and F. Tupin, "SAR-SIFT: A SIFT-like algorithm for applications on SAR images," in *Proc. IEEE IGARSS*, 2012, pp. 3478–3481.

[5] P. Schwind, S. Suri, P. Reinartz, and A. Siebert, "Applicability of the SIFT operator for geometrical SAR image registration," *Int. J. Remote Sens.*, vol. 31, no. 8, pp. 1959–1980, Mar. 2010.

[6] P. F. Alcantarilla, A. Bartoli, and A. J. Davison, "KAZE features," in *Proc. ECCV*, 2012, pp. 214–227.

[7] S. Wang, H. You, and K. Fu, "BFSIFT: A novel method to find feature matches for SAR image registration," *IEEE Geosci. Remote Sens. Lett.*, vol. 9, no. 4, pp. 649–653, Jul. 2012.

[8] L. P. Dorado-Muñoz, M. Vélez-Reyes, A. Mukherjee, and B. Roysam, "A vector SIFT detector for interest point detection in hyperspectral imagery," *IEEE Trans. Geosci. Remote Sens.*, vol. 50, no. 11, pp. 4521–4533, Nov. 2012.

[9] P. Pietro and J. Malik, "Scale-space and edge detection using anisotropic diffusion," *IEEE Trans. Pattern Anal. Mach. Intell.*, vol. 12, no. 7, pp. 629–639, Jul. 1990.

[10] J. Weickert, B. M. T. H. Romeny, and M. A. Viergever, "Efficient and reliable schemes for nonlinear diffusion filtering," *IEEE Trans. Image Process.*, vol. 7, no. 3, pp. 398–410, Mar. 1998.

[11] R. Fjortoft, A. Lopes, P. Marthon, and E. Cubero-Castan, "An optimal multiedge detector for SAR image segmentation," *IEEE Trans. Geosci. Remote Sens.*, vol. 36, no. 3, pp. 793–802, May 1998.

[12] J. Weickert, *Anisotropic Diffusion in Imaging Processing*. Stuttgart, Germany: B. G. Teubner, 1998.

[13] A. Wong and D. A. Clausi, "ARRSI: Automatic registration of remote-sensing images," *IEEE Trans. Geosci. Remote Sens.*, vol. 45, no. 5, pp. 1483–1493, May 2007.

[14] H. Goncalves, J. A. Goncalves, and L. Corte-Real, "Measures for an objective evaluation of the geometric correction process quality," *IEEE Geosci. Remote Sens. Lett.*, vol. 6, no. 2, pp. 292–296, Apr. 2009.